## Quantum backflow in biased tight-binding systems

Francisco Ricardo Torres Arvizu, Adrian Ortega, and Hernán Larralde\* Instituto de Ciencias Físicas, UNAM, Av. Universidad s/n,

ZIP 62210 Cuernavaca Morelos, México

2 Centro Universitario de Guadalajara,

Universidad de Guadalajara, Calle Guanajuato 1045,

ZIP 44160, Guadalajara, Jalisco, México

We study the phenomenon of quantum backflow in tight-binding systems with complex couplings, considering different boundary conditions and lattice sizes. Backflow is an intrinsically non-classical effect where the density flux associated with a particle described by the superposition of wave functions with, say, positive momentum, acquires negative values. We calculate the superposition of positive momentum states that gives rise to the strongest backflow in the systems. We also evaluate the bounds on the total amount of probability that flows in the opposite direction of the particle's momentum.

## I. INTRODUCTION

The phenomenon of backflow is a non-classical and non-linear effect that occurs when the probability current (or density flux) of a particle takes values opposite to its momentum. This phenomenon was first identified in 1969 by Allcock in the context of arrival times in quantum mechanics [1]. Bracken and Melloy [2] systematically formulated the problem in terms of the probability current of a normalized wave packet with positive momentum. The most significant outcome of their approach is that the total probability that flows in the direction opposite to the momentum is bounded by a universal constant  $c_{\rm BM}$ . The exact value of the constant  $c_{\rm BM}$  is unknown, with the best numerical estimates obtained in [3, 4], suggesting that in the infinite continuous case considered in those works,  $c_{\rm BM} \approx 0.0384517$ ; while, to the best of our knowledge, what occurs in discrete systems is not known. The phenomenon of backflow has been investigated in various extensions of the original

<sup>\*</sup> Email: hernan@icf.unam.mx

setup [5–8], including relativistic generalizations [9], scattering conditions [10], and manyparticle formulations [11]. Other systems that exhibit backflow have also been identified, for example in [12–14]. Continuing in this vein, it is natural to extend the study of this phenomenon to discrete versions of such systems, and explore how they differ from their continuous counterparts. In this work we focus on the nature of backflow in tight-binding chains with constant (complex) next nearest-neighbor couplings and onsite energies, which can be regarded as discrete analogues of a free-particle-type Hamiltonian [15]. The tightbinding model has traditionally been used to determine electronic and transport properties in solids with periodic potentials, such as insulators and semiconductors [16]. However, its versatility and simplicity have allowed it to be used to characterize a wide variety of analogous physical systems, ranging from waveguides [17–20] to quantum random walks [21, 22]. We consider both periodic and infinite chains, which can be related to the general backflow setups described in [23] and [2]. Interest in periodic systems arises from several characteristics, among them that the momentum eigenfunctions are normalizable and their spectrum is discrete, making the calculation of the flux bounds easier to a certain extent [23, 24. Generalizations using periodic boundary conditions have been used to study backflow in a variety of situations [25–28]. Extensions to two dimensional systems [29], where it turns out that the backflow is not bounded [30], have also been considered.

In what follows we address two questions that naturally arise in regards to this phenomenon, the first of which, somewhat surprisingly, has been rarely explored (see, for example, [28]). These are: How large can the backflowing probability density flux be? and second, along the lines of [2]: Is the total probability flowing backwards bounded? We consider tight-binding chains with complex couplings. Among other features [31], such models have attracted attention because, they break time-reversal symmetry while remaining Hermitian.

The outline of the paper is as follows: In Section II, we introduce the systems we will consider and present the solutions of the corresponding Schrödinger equations. In Section III, we determine the momentum operator associated with the system, with the aim of identifying the conditions under which its eigenvalues are positive, thereby enabling the construction of superpositions of states with strictly positive momentum. Section IV is devoted to the continuity equations and to the physical role of the imaginary part of the coupling constant in these systems. In Section V, we calculate the corresponding fluxes

and analyze the optimal bounds of the probability current, both for a simple superposition of two states with positive momentum, and then for general superpositions of such states. For completeness, in section VI, we undertake the "traditional" calculation of Bracken and Melloy [2, 23], which consists in the computation of the total probability flowing backwards at the origin during a time interval T, in order to estimate the constant  $c_{\rm BM}$ . Finally, our conclusions are summarized in Section VII.

#### II. THE MODELS AND THEIR SOLUTIONS

In this section we present the two configurations of the system under study and their corresponding solutions. This shall also help to fix the notation followed throughout the paper.

The tight-binding chain is described by the Hamiltonian (see figure fig.1):

$$\mathbf{H} = -\tau ((1 + i\epsilon)\mathbf{S} + (1 - i\epsilon)\mathbf{S}^{\dagger}), \tag{1}$$

where  $\tau$  is a coupling strength, which sets the energy scale of the problem, and  $\epsilon$  is a dimensionless parameter whose physical meaning will be discussed in Section IV. We are considering constant onsite energies, so without loss of generality, we can set these to zero. The Hamiltonian is written in the site basis and  $\mathbf{S}, \mathbf{S}^{\dagger}$  are shift operators: if a state is written in the site representation  $\psi_k(j)$ , the actions of these operators are [32, 33]

$$\mathbf{S}\psi_k(j) = \psi_k(j+1), \quad \mathbf{S}^{\dagger}\psi_k(j) = \psi_k(j-1). \tag{2}$$

The eigenstates state of the time-independent Schrödinger equation

$$E_k \psi_k(j) = -\tau ((1 + i\epsilon)\psi_k(j+1) + (1 - i\epsilon)\psi_k(j-1)), \tag{3}$$

are simply the plane-waves

$$\psi_k(j) = \frac{e^{ikj}}{\sqrt{2\pi}}. (4)$$

The energy corresponding to the eigenfunction  $\psi_k(j)$  is

$$E_k = -2\tau\sqrt{1+\epsilon^2}\cos\left(k+\xi\right),\tag{5}$$

where  $\xi = \arctan(\epsilon)$  and k represents the pseudo-momentum (c.f. Sec. III for the discussion of the physical momentum).

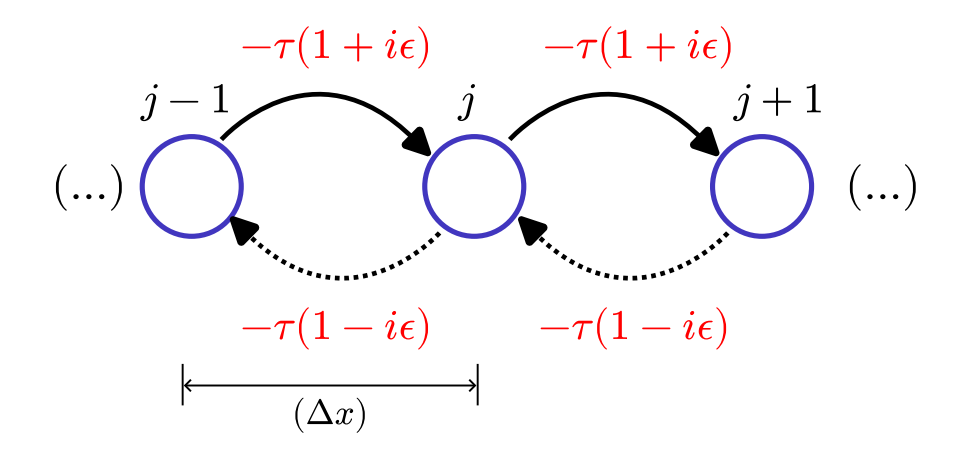


FIG. 1: Segment of the chain, the lattice elements are separated by a distance  $(\Delta x)$  and the nearest neighbor hopping is characterized by a complex number with imaginary part  $\pm \epsilon$ .

For the periodic chain with N sites the time-independent Schrödinger equation, its solutions (up to a normalization constant), and the corresponding energies are essentially the same as for the infinite chain with  $k(n) = \frac{2n\pi}{N}$ , where n is an integer so the eigenfunction  $\psi_{k(n)}(j)$  satisfies the boundary condition  $\psi_{k(n)}(0) = \psi_{k(n)}(N)$ .

#### III. THE MOMENTUM OPERATOR IN TIGHT-BINDING SYSTEMS

In this section, we determine the momentum operator  $\mathbf{p}$  of a tight-binding system in order to establish the values of the pseudo-momentum k for which the eigenvalues of the momentum operator are positive. This insures that the states in which there is backflow are composed only of superpositions of eigenstates with positive momentum.

We can write the momentum operator using the Heisenberg equation [34, 35],

$$\mathbf{p} = \mu \frac{\partial \mathbf{r}(\mathbf{t})}{\partial t} = \frac{\mu}{i\hbar} [\mathbf{r}(t), \mathbf{H}], \tag{6}$$

where  $\mu$  is the mass of the particle and the position takes the values  $(\Delta x)j$ , with j integer (see fig.1) [15, 36].

The time evolution of the position operator can be obtained using the Baker-Campbell-Hausdorff lemma [37]:

$$\mathbf{r}(t) = e^{i\mathbf{H}t/\hbar}\mathbf{r}e^{-i\mathbf{H}t/\hbar} = \mathbf{r} + [\mathbf{H}, \mathbf{r}]\frac{it}{\hbar} + [\mathbf{H}, [\mathbf{H}, \mathbf{r}]]\frac{(it/\hbar)^2}{2!} + [\mathbf{H}, [\mathbf{H}, \mathbf{r}]]\frac{(it/\hbar)^3}{3!} + \dots$$
(7)

Computing the commutators we obtain

$$[\mathbf{H}, \mathbf{r}] = -(\Delta x)\tau ((1 + i\epsilon)\mathbf{S} - (1 - i\epsilon)\mathbf{S}^{\dagger})$$
(8)

and

$$[\mathbf{H}, [\mathbf{H}, \mathbf{r}]] = 0. \tag{9}$$

The last expression means that momentum is a conserved quantity and shares eigenfunctions with the Hamiltonian. Using eqs. (6), (7) and (9) one obtains

$$\mathbf{r}(t) = \mathbf{r} + \frac{\mathbf{p}}{\mu}t. \tag{10}$$

As expected, this is the position operator for rectilinear motion, since the Hamiltonian is a discretization of a one dimensional system where the particle moves freely. The momentum operator is

$$\mathbf{p} = \frac{(\Delta x)\mu\tau}{i\hbar} \Big( (1+i\epsilon)\mathbf{S} - (1-i\epsilon)\mathbf{S}^{\dagger} \Big), \tag{11}$$

and its eigenvalue equation is

$$\mathbf{p}\psi_k(j) = \frac{2(\Delta x)\mu\tau\sqrt{1+\epsilon^2}}{\hbar}\sin(k+\xi)\psi_k(j). \tag{12}$$

This agrees with the well-known relation between energy (c.f. eq. (5)) and the momentum eigenvalue p for tight-binding systems [34, 38–40]

$$\frac{(\Delta x)\mu}{\hbar} \frac{\partial E}{\partial k} = \frac{2(\Delta x)\mu\tau\sqrt{1+\epsilon^2}}{\hbar} \sin\left(k+\xi\right). \tag{13}$$

From eq. (12) it can be seen that for the infinite chain, eigenstates with positive momenta occur when the following condition

$$k \in [-\xi, \ \pi - \xi] \tag{14}$$

is satisfied.

For the periodic chain the eigenstates with positive momentum will be those where

$$n \in \{\eta_1, \eta_1 + 1, \dots, \eta_2 - 1, \eta_2\},$$
 (15)

where  $\eta_1 = \left\lceil -\frac{\xi}{2\pi} N \right\rceil$  and  $\eta_2 = \left\lfloor \frac{\pi - \xi}{2\pi} N \right\rfloor$ . Here  $\lfloor x \rfloor$  and  $\lceil x \rceil$  denotes the usual floor and ceil functions.

## IV. CONTINUITY EQUATION

Given a wave function  $\Psi(j,t)$ , solution of the time dependent Schrödinger equation with Hamiltonian (1), the continuity equation for its probability density  $|\Psi(j,t)|^2$  reads

$$\frac{\partial}{\partial t} |\Psi(j,t)|^2 = -J(j+1,t) + J(j,t), \tag{16}$$

where J(j,t) is the flux from site j-1 to j, at time t, and is given by

$$J(j,t) = \frac{\tau}{i\hbar} \left( \Psi^*(j-1,t)\Psi(j,t) - \Psi(j-1,t)\Psi^*(j,t) + i\epsilon(\Psi^*(j-1,t)\Psi(j,t) + \Psi(j-1,t)\Psi^*(j,t)) \right). \tag{17}$$

To address the physical meaning of the parameter  $\epsilon$  we consider the continuous limit of eq. (16), which can be obtained by recalling that the position x is measured in terms of the fundamental length  $(\Delta x)$  through the relation  $x = (\Delta x)j$  [41]. Now, taking  $(\Delta x) \to 0$ , we can expand the wave function in Taylor series as

$$\Psi((\Delta x)(j\pm 1),t) \sim \Psi(x,t) \pm (\Delta x) \frac{\partial}{\partial x} \Psi(x,t) + \frac{(\Delta x)^2}{2} \frac{\partial^2}{\partial x^2} \Psi(x,t) + \dots, \tag{18}$$

Using eqs.(16) and (17), we obtain that the continuous expression of the flux is

$$J(x,t) = \frac{\hbar}{2\mu i} \left[ \Psi^*(x,t) \frac{\partial}{\partial x} \Psi(x,t) - \Psi(x,t) \frac{\partial}{\partial x} \Psi^*(x,t) + 2i\zeta |\Psi(x,t)|^2 \right], \tag{19}$$

where the constants  $\tau$  and  $\epsilon$  are chosen as:

$$\tau = \frac{\hbar^2}{2\mu(\Delta x)^2}, \qquad \epsilon = \zeta(\Delta x), \tag{20}$$

consistently with the finite-difference approximation [15, 42].

The first terms on the RHS of eq.(19) are the "standard" probability flux of a quantum particle, while the last can be identified as a "drift" term, much like what happens in biased diffusion [41]. Applying the same approximations to the Hamiltonian in eq.(1) yields the time dependent Schrödinger equation

$$i\hbar \frac{\partial}{\partial t} \Psi(x,t) = -\left(\frac{\hbar^2}{2\mu} \frac{\partial^2}{\partial x^2} + i \frac{\zeta \hbar^2}{\mu} \frac{\partial}{\partial x}\right) \Psi(x,t), \tag{21}$$

where we omitted an irrelevant constant energy term.

A physical realization of a quantum system with such a drift can be obtained, for example, by considering the Hamiltonian of a free particle confined to a ring in the xy plane with radius  $r_0$ , centered at the origin, in the presence of a constant magnetic field of the form  $\vec{B} = B_0 \hat{z}$  [43]. The Hamiltonian for a free particle in an external magnetic field reads

$$\mathbf{H} = \frac{1}{2\mu} \left( \mathbf{p} - eA\mathbb{I} \right)^2, \tag{22}$$

where e is the charge of the particle,  $\mathbb{I}$  is the identity operator, and for this system,  $\mathbf{p}$  can be written as

$$\mathbf{p} = \frac{p_{\vartheta}}{r_0} \,\hat{\vartheta},\tag{23}$$

with  $p_{\vartheta}$  being the momentum associated with the angular coordinate, which can be identified as the angular momentum.

For the magnetic field  $\vec{B}$ , the corresponding vector potential can be written as

$$\vec{A} = -r_0 B_0 \hat{\vartheta}. \tag{24}$$

Thus, the Hamiltonian becomes

$$\mathbf{H} = \frac{1}{2\mu} \left( \frac{\mathbf{L}_{\mathbf{z}}}{r_0} + e r_0 B_0 \mathbb{I} \right)^2, \tag{25}$$

where the operator  $\mathbf{L}_z$  is defined as usual by  $\mathbf{L}_z = -i\hbar \frac{\partial}{\partial \vartheta}$ . The term proportional to  $B_0^2$ , after expanding the square, produces an irrelevant constant energy offset which can be ignored, so the Hamiltonian eq. (25) reduces to

$$\mathbf{H}' = -\frac{\hbar^2}{2\mu} \left( \frac{1}{r_0^2} \frac{\partial^2}{\partial \theta^2} + i \frac{eB_0}{\hbar} \frac{\partial}{\partial \theta} \right). \tag{26}$$

This is the Hamiltonian of a rigid rotor in a magnetic field [43], which is analogous to the Hamiltonian in equation (21), and can be regarded as the continuous counterpart of the Hamiltonian in eq. (1) with periodic boundary conditions.

A different interpretation is reached recalling that appearance of the drift term in diffusive systems can be associated with a moving reference frame, in which case such term can be eliminated by means of a simple Galilean transformation. It is easy to see that with the transformation [44, 45]

$$x' = x - \frac{\hbar \zeta}{\mu} t, \qquad t' = t. \tag{27}$$

in the time dependent Schrodinger equation eq. (21), we get rid of the drift-like flux and recover the standard quantum flux. The drift is also affects in the energy and momentum, as shown in expressions (5) and (12); and has the effect of changing the range of pseudomomentum values k that correspond to states with positive momentum, as shown in eq. (14).

# V. MAXIMAL BACKFLOW AND BOUNDS ON PROBABILITY DENSITY FLOW

In this section we construct superpositions of states with positive momenta to study the appearance of backflow and determine the cases that maximize the effect. First, we explore

the phenomenon in a two state superposition, and then analyze the phenomenon in general superpositions involving all possible states with positive momentum.

## A. An illustrative example: The two-state backflow

We consider a wave function  $\Psi(j,t)$  comprised by two eigenstates  $\psi_{k(m_1)}(j,t)$  and  $\psi_{k(m_2)}(j,t)$  with  $m_1, m_2$  belonging to the set of eq. (15) so  $\Psi(j,t)$  is the simplest superposition of eigenstates that have positive momentum:

$$\Psi(j,t) = \frac{\cos\left(\frac{\theta}{2}\right)e^{i\left(\frac{2\pi m_1 j}{N} - \frac{E_{m_1}}{\hbar}t\right)} + \sin\left(\frac{\theta}{2}\right)e^{i\left(\frac{2\pi m_2 j}{N} - \frac{E_{m_2}}{\hbar}t + \gamma\right)}}{\sqrt{N}},\tag{28}$$

where  $\theta \in [0, \pi]$  and  $\gamma \in [0, 2\pi]$ .

The flux computed via eq. (17) is

$$J(j,t) = \frac{2\tau\sqrt{1+\epsilon^2}}{N\hbar} \left[ \cos\left(\frac{(m_1-m_2)\pi}{N}\right) \sin\left(\frac{(m_1+m_2)\pi}{N}+\xi\right) + \cos(\theta) \sin\left(\frac{(m_1-m_2)\pi}{N}\right) \cos\left(\frac{(m_1+m_2)\pi}{N}+\xi\right) + \cos\left(\frac{(2j-1)(m_1-m_2)\pi}{N}-\frac{E_{m_1}-E_{m_2}}{\hbar}t-\gamma\right) \sin\left(\frac{(m_1+m_2)\pi}{N}+\xi\right) \sin(\theta) \right],$$

$$(29)$$

Note that the term  $\sin\left(\frac{(m_1+m_2)\pi}{N}+\xi\right)$  always takes positive values for the current election of  $m_1$  and  $m_2$ . This can be seen by assuming, without loss of generality, that  $m_1 < m_2$ , then  $m_1 \le \frac{m_1+m_2}{2} \le m_2$ , so  $\frac{(m_1+m_2)\pi}{N}$  corresponds to a point between the bounds of the set defined in eq. (15). Thus, the minimum of the flux for a given j and  $\gamma$  fixed, is reached at times t such that the cosine factor in which t appears is -1, that is

$$\mathcal{J}(\theta) = \min_{\{t\}} (J(j,t)) = \frac{2\tau\sqrt{1+\epsilon^2}}{N\hbar} \left[ \cos\left(\frac{(m_1 - m_2)\pi}{N}\right) \sin\left(\frac{(m_1 + m_2)\pi}{N} + \xi\right) + \cos(\theta) \sin\left(\frac{(m_1 - m_2)\pi}{N}\right) \cos\left(\frac{(m_1 + m_2)\pi}{N} + \xi\right) - \sin\left(\frac{(m_1 + m_2)\pi}{N} + \xi\right) \sin(\theta) \right].$$
(30)

Now we can adjust the parameter  $\theta$  to obtain the minimum flux given the two states with positive momenta. First, we rewrite the last equation as

$$\mathcal{J}(\theta) = \frac{2\tau\sqrt{1+\epsilon^2}}{N\hbar}(a+b\cos(\theta)-c\sin(\theta)),\tag{31}$$

where

$$a = \cos\left(\frac{(m_1 - m_2)\pi}{N}\right) \sin\left(\frac{(m_1 + m_2)\pi}{N} + \xi\right),$$

$$b = \sin\left(\frac{(m_1 - m_2)\pi}{N}\right) \cos\left(\frac{(m_1 + m_2)\pi}{N} + \xi\right),$$

$$c = \sin\left(\frac{(m_1 + m_2)\pi}{N} + \xi\right).$$
(32)

Minimizing the expression of eq. (31) with respect to  $\theta$ , we find that

$$\tan(\theta) = -\frac{c}{b},\tag{33}$$

Thus, the global minimum of J(j,t) is

$$\min_{\{t,\theta\}}(J(j,t)) = \frac{2\tau\sqrt{1+\epsilon^2}}{N\hbar}(a - \sqrt{b^2 + c^2}).$$
 (34)

Note that  $a < \sqrt{b^2 + c^2}$  as long as  $m_1 \neq m_2$ , so the lowest flux attainable from the superposition of plane waves with positive momenta is, indeed, negative.

## B. Infinite chain

We now generalize the procedure from the previous section to a superposition that includes all eigenstates of the infinite chain with positive momentum, with the aim of determining the lower and upper bounds that constrain the probability density flux.

For this system, according to eq. (14), the most general superposition of states with positive momenta is

$$\psi(j,t) = \frac{1}{\sqrt{2\pi}} \int_{-\xi}^{\pi-\xi} e^{i\left(kj - \frac{E_k}{\hbar}t\right)} \phi(k) \, dk. \tag{35}$$

Here  $\phi(k)$  is a weight function that satisfies the normalization condition

$$\int_{-\xi}^{\pi-\xi} |\phi(k)|^2 \, dk = 1. \tag{36}$$

The flux associated to the wave function  $\psi(j,t)$  in eq. (35) can be computed from eq.(17) as a functional of  $\phi(k)$ :

$$J(j,t) = \frac{\tau\sqrt{1+\epsilon^2}}{\pi\hbar} \int_{-\xi}^{\pi-\xi} \int_{-\xi}^{\pi-\xi} \phi^*(k')\phi(k) e^{i\left((j-\frac{1}{2})(k-k') + \frac{(E_{k'}-E_k)t}{\hbar}\right)} \sin\left(\frac{k+k'}{2} + \xi\right) dk dk',$$
(37)

We want to minimize the flux at a given position j' and time t', subject to the constraint of eq. (36). To do this, we define the functional

$$I_{1}(\phi^{*}(k'),\phi(k)) = \frac{\tau\sqrt{1+\epsilon^{2}}}{\pi\hbar} \int_{-\xi}^{\pi-\xi} \int_{-\xi}^{\pi-\xi} \phi^{*}(k')\phi(k) e^{i\left((j'-\frac{1}{2})(k-k') + \frac{(E_{k'}-E_{k})t'}{\hbar}\right)} \sin\left(\frac{k+k'}{2} + \xi\right) dk \, dk' - \lambda \int_{-\xi}^{\pi-\xi} |\phi(k')|^{2} \, dk'}, \tag{38}$$

where  $\lambda$  is a Lagrange multiplier. From this expression, the following Euler-Lagrange equation can be derived:

$$\frac{\tau\sqrt{1+\epsilon^2}}{\pi\hbar} \int_{-\xi}^{\pi-\xi} \phi(k) \, e^{i\left((j'-\frac{1}{2})(k-k') + \frac{(E_{k'}-E_k)t'}{\hbar}\right)} \sin\left(\frac{k+k'}{2} + \xi\right) \, dk' = \lambda\phi(k'),\tag{39}$$

or

$$\frac{\tau\sqrt{1+\epsilon^2}}{\pi\hbar} \int_{-\xi}^{\pi-\xi} \phi(k) \, e^{i \left((j'-\frac{1}{2})(k-k') + \frac{(E_{k'}-E_k)t'}{\hbar}\right)} \left[\sin\left(\frac{k+\xi}{2}\right)\cos\left(\frac{k'+\xi}{2}\right) + \cos\left(\frac{k'+\xi}{2}\right)\sin\left(\frac{k'+\xi}{2}\right)\right] dk = \lambda\phi(k'), \tag{40}$$

The last equation is a homogeneous Fredholm integral equation that can be solved by direct computation [46]. First we set

$$\int_{-\xi}^{\pi-\xi} \phi(k) e^{i(k(j'+\frac{1}{2})+t'\tau\sqrt{1+\epsilon^2}\cos(k+\xi))} \sin\left(\frac{k+\xi}{2}\right) dk = \alpha, \tag{41}$$

$$\int_{-\xi}^{\pi-\xi} \phi(k) e^{i(k(j'+\frac{1}{2})+t'\tau\sqrt{1+\epsilon^2}\cos(k+\xi))} \cos\left(\frac{k+\xi}{2}\right) dk = \beta, \tag{42}$$

thus,

$$\lambda \,\phi(k') = e^{-i(k'(j'+\frac{1}{2})+t'\tau\sqrt{1+\epsilon^2}\cos(k'+\xi))} \left[ \alpha \cos\left(\frac{k'+\xi}{2}\right) + \beta \sin\left(\frac{k'+\xi}{2}\right) \right]. \tag{43}$$

Substituting this expression in eqs. (41) and (42), and evaluating the integrals, gives the following eigenvalue equation

$$\frac{\sqrt{1+\epsilon^2}\tau}{\pi\hbar} \begin{bmatrix} 1 & \frac{\pi}{2} \\ \frac{\pi}{2} & 1 \end{bmatrix} \begin{bmatrix} \alpha \\ \beta \end{bmatrix} = \lambda \begin{bmatrix} \alpha \\ \beta \end{bmatrix}, \tag{44}$$

from which we can compute  $\lambda$ 

$$\lambda_{\pm} = \frac{(2 \pm \pi)\sqrt{1 + \epsilon^2}\tau}{2\hbar\pi},\tag{45}$$

then, we have that

$$\alpha = \pm \beta. \tag{46}$$

We normalize the weight function  $\phi(k')$  in eq. (43) by choosing

$$\beta = \frac{1}{\sqrt{\pi \pm 2}},\tag{47}$$

so we find

$$\phi_{\pm}(k') = \frac{e^{-i(k'(j' + \frac{1}{2}) + \frac{t'\tau}{\hbar}\sqrt{1 + \epsilon^2}\cos(k' + \xi))}}{\sqrt{\pi \pm 2}} \left[ \pm \cos\left(\frac{k' + \xi}{2}\right) + \sin\left(\frac{k' + \xi}{2}\right) \right]. \tag{48}$$

The flux is then given by

$$J(j;j',t;t') = \frac{\tau\sqrt{1+\epsilon^2}}{\pi(\pi\pm 2)\hbar} \int_{-\xi}^{\pi-\xi} \int_{-\xi}^{\pi-\xi} e^{i((k-k')(j-j')+\sqrt{1+\epsilon^2}\tau(t-t')(\cos(k+\xi))-\cos(k'+\xi)))}$$

$$\left(\pm\cos\left(\frac{k'+\xi}{2}\right)+\sin\left(\frac{k'+\xi}{2}\right)\right)\left(\pm\cos\left(\frac{k+\xi}{2}\right)+\sin\left(\frac{k+\xi}{2}\right)\right)\sin\left(\frac{k+k'}{2}+\xi\right)dk\,dk'.$$

$$(49)$$

In fig. 2a, we illustrate the probability density flux given by Eq. (49) as a function of time for position j = j' = 3 compared to adjacent sites j - 1, j + 1, taking t' = 3, so the extreme values of the flux occur at site j = 3 at time t = 3 as observed. We also show the bounds associated with the corresponding eigenvalues  $\lambda_{\pm}$ . The insets show that the largest (smallest) flux values indeed coincide with the upper (lower) bounds at the correct positions and times, as expected.

#### C. Periodic chain

We address now the case when the system has periodic boundary conditions. A general state with nonnegative momentum can be written as the linear combination

$$\Psi(j,t) = \sum_{n=n_1}^{\eta_2} c_n a_n(j,t) = \frac{1}{\sqrt{N}} \sum_{n=n_1}^{\eta_2} e^{i\left(\frac{2\pi nj}{N} - E_n t\right)} c_n, \tag{50}$$

remembering that  $\eta_2 = \lfloor \frac{\pi - \xi}{2\pi} N \rfloor$  and  $\eta_1 = \lceil -\frac{\xi}{2\pi} N \rceil$ . With these sumation limits, we are taking under consideration all the nonnegative possible flux states, as we discussed in the previous section. The coefficients  $c_m$  satisfy the normalization condition

$$\sum_{n=\eta_1}^{\eta_2} |c_n|^2 = 1. (51)$$

The flux can be found using eq. (17), i.e.

$$J(j,t) = \frac{2\tau\sqrt{1+\epsilon^2}}{N\hbar} \sum_{n=\eta_1}^{\eta_2} \sum_{m=\eta_1}^{\eta_2} c_m^* c_n e^{i\left(\frac{(2j-1)(m-n)\pi}{N} - \frac{(E_n - E_m)t}{\hbar}\right)} \sin\left(\frac{(m+n)\pi}{N} + \xi\right).$$
 (52)

The derivation of the bounds is analogous to the infinite-chain case; however, instead of finding a function, we seek to determine the sequence  $c_m$  that extremizes eq. (52) (see the Appendix for details). Here again we have  $\max(J(j,t)) = \lambda_+$  and  $\min(J(j,t)) = \lambda_-$  where

$$\lambda_{\pm} = \frac{\tau\sqrt{1+\epsilon^2}}{N\hbar} \left[ \csc\left(\frac{\pi}{N}\right) \sin\left(\frac{\pi(\eta_2+1-\eta_1)}{N}\right) \sin\left(\frac{\pi(\eta_1+\eta_2)}{N}+\xi\right) \right. \\ \left. \pm \sqrt{(\eta_2+1-\eta_1)^2 - \left(\cos\left(\frac{\pi(\eta_1+\eta_2)}{N}+\xi\right) \csc\left(\frac{\pi}{N}\right) \sin\left(\frac{\pi(\eta_2+1-\eta_1)}{N}\right)\right)^2} \right].$$
 (53)

The corresponding sequences associated with  $\lambda_{\pm}$  are

$$c_{m}^{\pm} = \aleph_{\pm} e^{-i\left(\frac{(2j'-1)m\pi}{N} - \frac{E_{m}t'}{\hbar}\right)} \left[\pm\sqrt{\eta_{2}+1-\eta_{1}-\cos\left(\frac{\pi(\eta_{1}+\eta_{2})}{N}+\xi\right)\csc\left(\frac{\pi}{N}\right)\sin\left(\frac{\pi(\eta_{2}+1-\eta_{1})}{N}\right)}\cos\left(\frac{m}{N}\pi + \frac{\xi}{2}\right) + \sqrt{\eta_{2}+1-\eta_{1}+\cos\left(\frac{\pi(\eta_{1}+\eta_{2})}{N}+\xi\right)\csc\left(\frac{\pi}{N}\right)\sin\left(\frac{\pi(\eta_{2}+1-\eta_{1})}{N}\right)}\sin\left(\frac{m}{N}\pi + \frac{\xi}{2}\right)\right],$$

$$(54)$$

where  $\mathcal{N}_{\pm}$  is a normalization constant given by  $\mathcal{N}_{\pm} = \frac{1}{\sqrt{\mathcal{D}_{\pm}}}$  with

$$\begin{split} & \mathcal{D}_{\pm} \! = \! \left(\eta_2 + 1 - \eta_1\right)^2 - \cos^2\!\left(\frac{\pi(\eta_1 \! + \! \eta_2)}{N} + \xi\right) \csc^2\!\left(\frac{\pi}{N}\right) \sin^2\!\left(\frac{\pi(\eta_2 \! + \! 1 \! - \! \eta_1)}{N}\right) \\ & \pm \csc\!\left(\frac{\pi}{N}\right) \sin\!\left(\frac{\pi(\eta_2 \! + \! 1 \! - \! \eta_1)}{N}\right) \! \sqrt{(\eta_2 \! + \! 1 \! - \! \eta_1)^2 \! - \! \cos^2\!\left(\frac{\pi(\eta_1 \! + \! \eta_2)}{N} \! + \! \xi\right) \csc^2\!\left(\frac{\pi}{N}\right) \sin^2\!\left(\frac{\pi(\eta_2 \! + \! 1 \! - \! \eta_1)}{N}\right)} \sin\!\left(\frac{\pi(\eta_1 \! + \! \eta_2)}{N} \! + \! \xi\right) . \end{split}$$

In fig. 2b, we show the flux computed through Eq. (52) for the sequence defined in Eq. (54), together with their respective bounds  $\lambda_{\pm}$ , using the same values of j' and t' as in the infinite chain. The main difference with respect to that case lies in the fact that J(j; j', t; t') does not decay to zero as t approaches infinity; instead, it oscillates with smaller amplitudes, exhibiting intervals of attenuation and amplification, although it does not appear to reach the same magnitude as at j' and t'.

The case  $\epsilon = 0$  simplifies considerably. In this situation,  $\eta_1 = 0$  and we take  $\eta_2$  as follows

$$\eta_2 = \begin{cases} \frac{N}{2} - 1, & \text{for } N \text{ even} \\ \frac{N-1}{2}, & \text{for } N \text{ odd} \end{cases}$$

The choice of  $\eta_2$  for odd N is made in order to avoid the zero-moment state being considered twice in the state of eq. (35). Thus the bounds of the flux given in eq.(53) become

$$\lambda_{\pm} = \begin{cases} \frac{\tau}{N\hbar} \left( \cot\left(\frac{\pi}{N}\right) \pm \sqrt{\frac{N^2}{4} - 1} \right), & \text{for } N \text{ even} \\ \frac{\tau}{2N\hbar} \left( \cot\left(\frac{\pi}{2N}\right) \pm \sqrt{N(N+2)} \right), & \text{for } N \text{ odd} \end{cases}$$
 (55)

Thus we have that eq. (54) reduces to

$$c_{m}^{\pm} = \begin{cases} \frac{e^{-i\left(\frac{(2j'-1)m\pi}{N} - \frac{E_{m}t'}{h}\right)}}{\sqrt{\frac{1}{2}\left[N^{2} - 2 \pm 2\sqrt{N^{2} - 4}\cot\left(\frac{\pi}{N}\right)\right]}} \left[\pm\sqrt{N} - 2\cos\left(\frac{m}{N}\pi\right) + \sqrt{N} + 2\sin\left(\frac{m}{N}\pi\right)\right], & \text{for } N \text{ even} \\ \frac{e^{-i\left(\frac{(2j'-1)m\pi}{N} - \frac{E_{m}t'}{h}\right)}}{\sqrt{\frac{1}{2}\left[(N+1)^{2} \pm \sqrt{N(N+2)}\cot\left(\frac{\pi}{2N}\right)\right]}} \left[\pm\sqrt{N}\cos\left(\frac{m}{N}\pi\right) + \sqrt{N+2}\sin\left(\frac{m}{N}\pi\right)\right], & \text{for } N \text{ odd.} \end{cases}$$

$$(56)$$

The effect of the parameter  $\epsilon$  on the probability density flux is shown in fig. (3). We observe that the magnitude of the bounds on the flux increases with  $\epsilon$ . This increase is more pronounced with  $\lambda_+$ , while it is comparatively milder with  $\lambda_-$ . An additional effect of the bias can be observed for the periodic chain, which exhibits larger oscillations of the flux far from the vicinity of t = t', and these oscillations also increase with  $\epsilon$ .

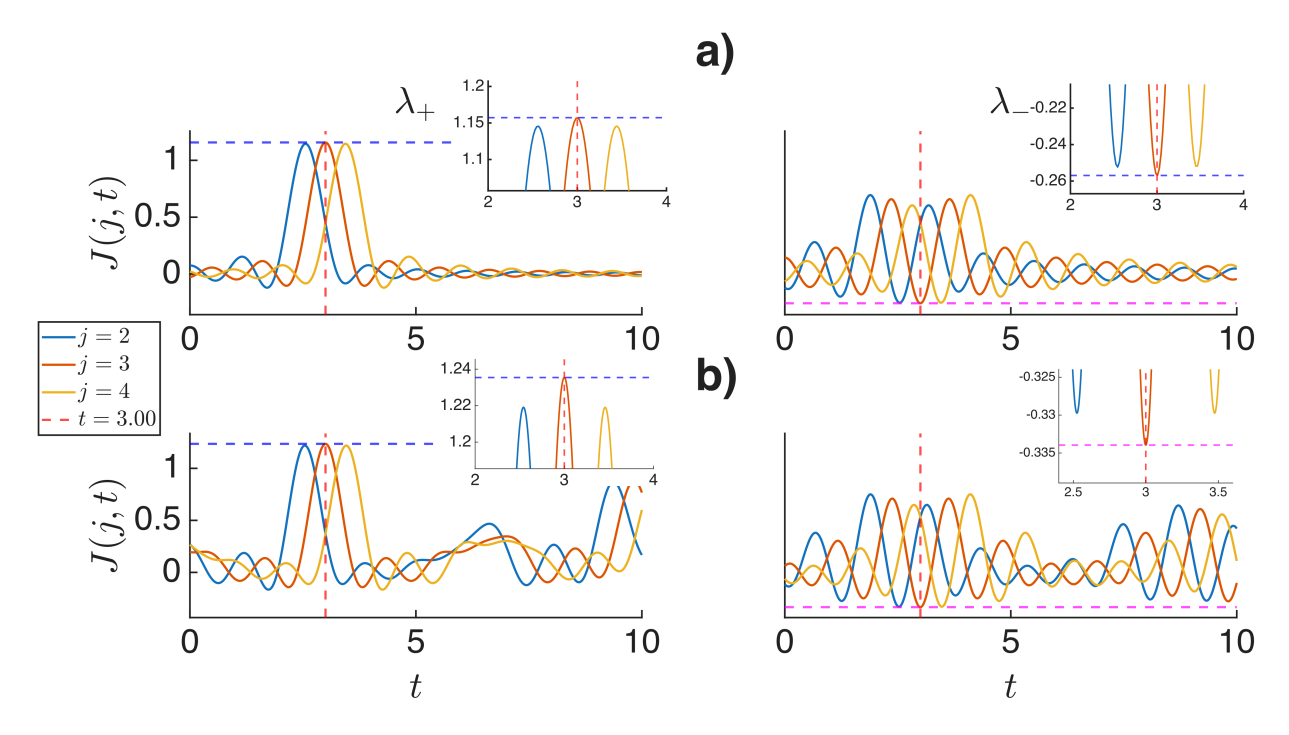


FIG. 2: The extreme values of the probability density flux as a at j'=3, and the nearest sites are shown as a function of t taking t'=3 (dashed red line), for the infinite chain (a) and the periodic chain (b) with  $\epsilon=1$  and N=9. We compute the flux using the function  $\phi_{\pm}(k)$  (sequence  $c_m^{\pm}$ ) and the bound associated :  $\lambda_+$  (blue dashed line) and  $\lambda_-$  (magenta dashed line).

## VI. THE BRACKEN-MELLOY APPROACH TO BACKFLOW

In this section we study backflow using the approach proposed by Bracken and Melloy. The original idea behind this procedure was formulated for a wave function composed by the superposition of states with positive momenta, as above, on a continuous, infinite one dimensional system. However, instead of calculating the extreme values of the flux, it aims to estimate the maximum amount of probability transferred from right to left of the origin, in a time interval T. This quantity can be defined as:  $c_{\rm BM} = {\rm max}\left(P(T) - P(0)\right)$ , where P(t) denotes the probability of finding the particle in the region, say, x < 0, after a time t [2]. This is equivalent to finding the upper bound of the integral of the flux over a time window [-T/2, T/2], at a given point (normally the origin), i.e.  $c_{\rm BM} = {\rm max}\left(-\int_{-T/2}^{T/2} J(0,t) \, dt\right)$ . It is important to point out that for systems with periodic boundary conditions only the second definition of  $c_{\rm BM}$  makes sense.

It has been shown that for continuous periodic systems, the total probability that flows

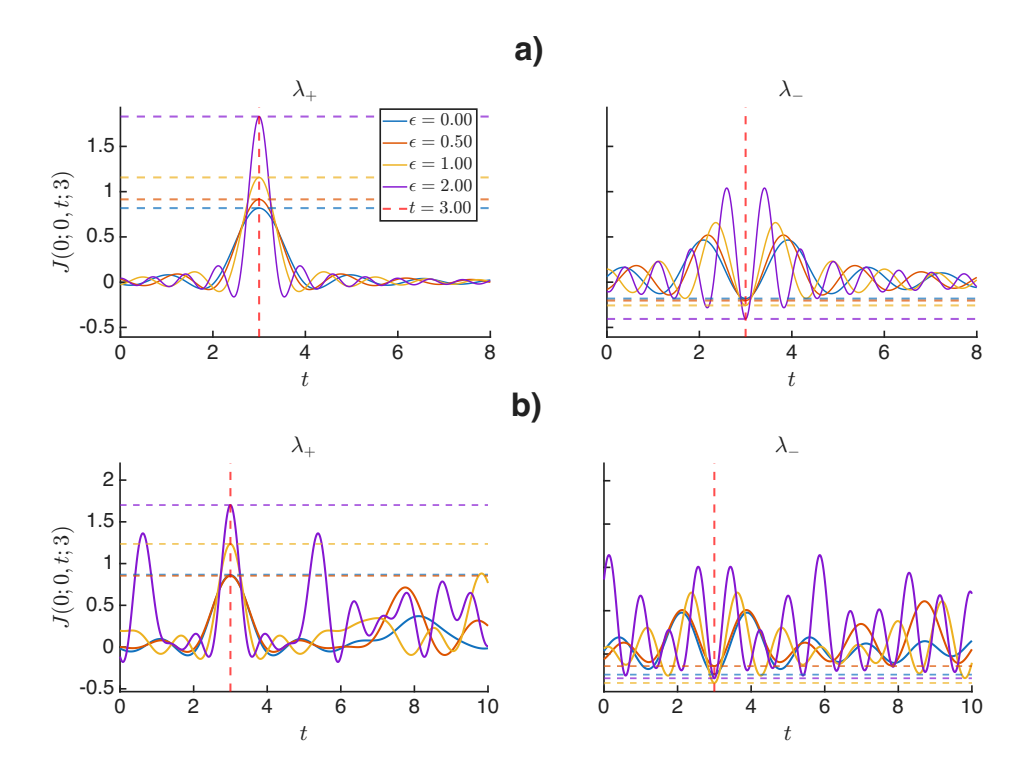


FIG. 3: The extreme values of the probability density flux for different  $\epsilon$  values at j' = 0, and t' = 3 (dashed red line) as a time function, for the infinite chain (a) and the periodic chain with N = 9 (b). The dashed lines are the respective bounds,  $\lambda_+$  and  $\lambda_-$  for the corresponding values of  $\epsilon$ .

to the left at the origin is bounded by  $c_{\rm ring}^{\rm cont} \approx 3.0380 c_{\rm BM}$  [23].

### A. Infinite chain

Here we proceed to derive the eigenvalue problem to maximize the integral  $-\int_{-T/2}^{T/2} J(0,t) dt$  for the infinite chain. First, we write the flux in eq. (37) at the origin as

$$J(0,t) = \frac{\tau\sqrt{1+\epsilon^2}}{\pi\hbar} \int_{-\xi}^{\pi-\xi} \int_{-\xi}^{\pi-\xi} \Phi^*(k')\Phi(k) e^{i\left(\frac{(E_{k'}-E_k)t}{\hbar}\right)} \sin\left(\frac{k+k'}{2}+\xi\right) dk dk', \qquad (57)$$

where  $\Phi(k) = e^{-i\frac{k}{2}}\phi(k)$ . Integrating over a temporal window [-T/2,T/2] we obtain

$$\int_{-T/2}^{T/2} J(0,t)dt = \int_{-\xi}^{\pi-\xi} \int_{-\xi}^{\pi-\xi} \frac{\sin\left(2\nu\sqrt{1+\epsilon^2}\sin\left(\frac{k+k'}{2}+\xi\right)\sin\left(\frac{k-k'}{2}\right)\right)}{2\pi\sin\left(\frac{k-k'}{2}\right)} \Phi^*(k')\Phi(k)dkdk', \quad (58)$$

where we introduced the adimensional parameter  $\nu = \frac{\tau T}{\hbar}$ . In order to maximize this quantity subject to the constraint given by eq. (36), we consider the functional:

$$I_{2}(\Phi(k), \Phi^{*}(k')) = -\int_{-\xi}^{\pi-\xi} \int_{-\xi}^{\pi-\xi} \Phi^{*}(k')\Phi(k) \frac{\sin\left(2\nu\sqrt{1+\epsilon^{2}}\sin\left(\frac{k+k'}{2}+\xi\right)\sin\left(\frac{k-k'}{2}\right)\right)}{2\pi\sin\left(\frac{k-k'}{2}\right)} dk dk'$$

$$-\lambda_{p} \int_{-\xi}^{\pi-\xi} |\Phi(k')|^{2} dk',$$
(59)

where  $\lambda_p$  is a Lagrange multiplier. Thus, we require the solution to the Euler-Lagrange equation:

$$\frac{1}{\pi} \int_{-\xi}^{\pi-\xi} \Phi(k) K(k, k') dk = \lambda_p \Phi(k'), \tag{60}$$

where the kernel K(k, k') is given by

$$K(k, k') = -\frac{\sin\left(2\nu\sqrt{1+\epsilon^2}\sin\left(\frac{k+k'}{2}+\xi\right)\sin\left(\frac{k-k'}{2}\right)\right)}{2\sin\left(\frac{k-k'}{2}\right)},\tag{61}$$

The continuous counterpart of the eigenvalue problem in Eq. (60) can be obtained through the following rescaling relations:  $k = (\Delta x)p$  and  $k' = (\Delta x)q$ . This leads to  $\sin((\Delta x)p) \sim p(\Delta x) + o((\Delta x)^2)$ . Writing  $\tau$  as in eq. (20), we have  $\nu = \frac{\hbar T}{2\mu(\Delta x)^2}$ . Taking the limit  $(\Delta x) \to 0$ we obtain

$$-\frac{1}{\pi} \int_{-\zeta}^{\infty} \tilde{\Phi}(p) \frac{\sin\left(\frac{T}{4\mu\hbar}(p+q+\zeta)(p-q)\right)}{p-q} dp = \lambda \,\tilde{\Phi}(q), \tag{62}$$

where  $\Phi(p) = \lim_{(\Delta x)\to 0} \Phi((\Delta x)p)$  and  $\zeta$  is defined in eq. (20). This is the "biased" version of the eigenvalue problem obtained by Bracken and Melloy [2].

Note that the kernel is the same as the one obtained for a backflow problem under a constant force [6, 7] with the difference that the lower integration limit in eq. (62) is shifted due to the effect of the drift.

As occurs with its continuous counterpart, the eigenvalue problem of eq. (60) cannot be computed analytically, so we approach the problem numerically. We base the calculation on the fact that the integration can be approximated as a symmetric finite square matrix acting on a vector. The largest eigenvalue of the matrix is taken as an approximation to  $\lambda_p$  [2–4]. Fig. (4) shows the dependence of the largest eigenvalue on the parameter  $\nu$  for several values of  $\epsilon$ . The value of  $\epsilon_{\rm BM}$ , which bounds the continuous case, is indicated in the figure. We observe that as  $\nu$  increases,  $\lambda_p$  appears to become bounded from below by  $\epsilon_{\rm BM}$ . Here,  $\epsilon$  appears to act only as some kind of scaling factor for each curve, narrowing it towards the y-axis without actually affecting qualitatively the behavior of the curves.

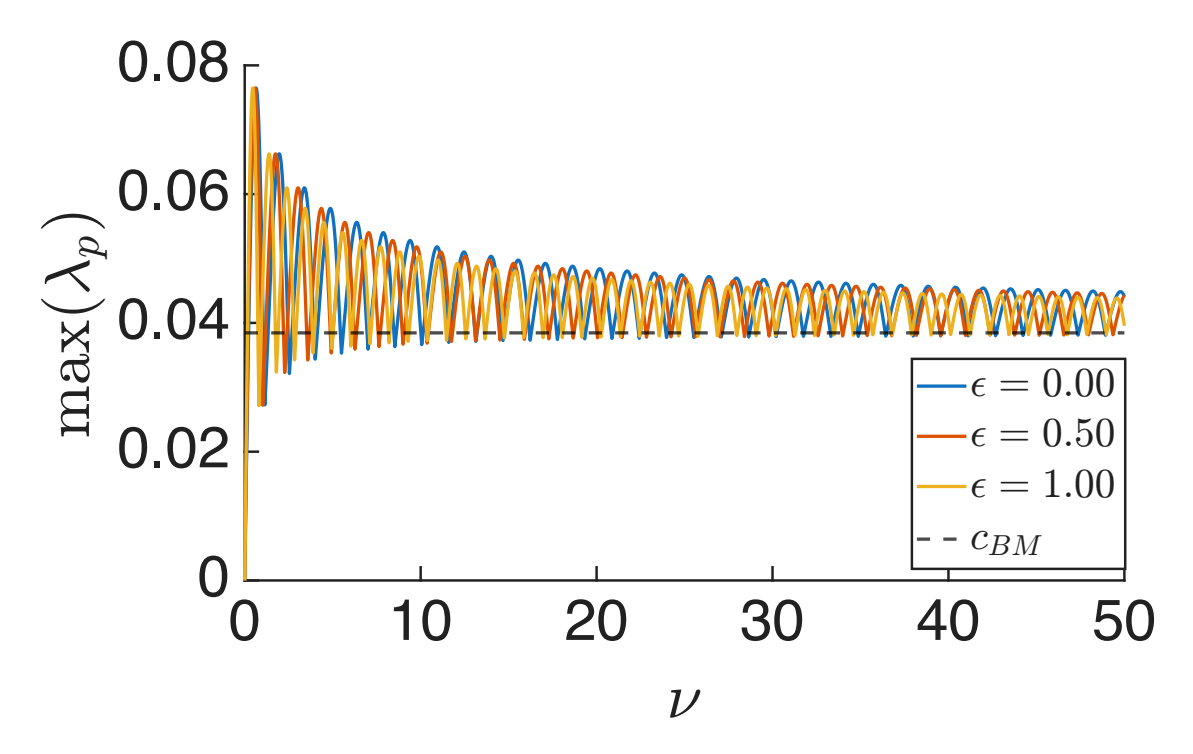


FIG. 4: Supremum of the minus time-integrated probability flux,  $\min(\lambda_p)$ , as a function of  $\nu$  for different values of  $\epsilon$ . It can be observed that  $\lambda_p$  appears to become bounded below by  $c_{\rm BM}$  as  $\nu \to \infty$ . The maximum of  $\lambda_p$  tends to be larger for values of  $\nu$  close to zero, and the effect of  $\epsilon$  does not significantly change the qualitative behavior of the curves. We found that the three curves reach a maximum value of 0.0764734.

## B. Periodic chain

In this section we consider the case of a periodic chain. First, as above, we compute the integral of eq. (51) at j = 0, over the temporal window [-T/2, T/2]:

$$\int_{-T/2}^{T/2} J(0,t) dt = \sum_{n=\eta_1}^{\eta_2} \sum_{m=\eta_1}^{\eta_2} C_m^* C_n \frac{\sin\left(2\nu\sqrt{1+\epsilon^2}\sin\left(\frac{(m+n)\pi}{N}+\xi\right)\sin\left(\frac{(m-n)\pi}{N}\right)\right)}{N\sin\left(\frac{(m-n)\pi}{N}\right)}.$$
 (63)

where  $C_n = e^{-\frac{in\pi}{N}}c_n$ . The extremes of this integral subject to the constraint eq. (51) can be found through the functional,

$$I_{2}(C_{m}^{*},C_{n}) = -\sum_{n=\eta_{1}}^{\eta_{2}} \sum_{m=\eta_{1}}^{\eta_{2}} C_{m}^{*} C_{n} \frac{e^{\frac{i(m-n)\pi}{N}} \sin\left(2\nu\sqrt{1+\epsilon^{2}}\sin\left(\frac{(m+n)\pi}{N}+\xi\right)\sin\left(\frac{(m-n)\pi}{N}\right)\right)}{N\sin\left(\frac{(m-n)\pi}{N}\right)} - \lambda_{p} \sum_{m=\eta_{1}}^{\eta_{2}} |C_{m}|^{2}.$$
 (64)

The Euler-Lagrange equation associated with eq. (64) leads to the eigenvalue equation

$$\sum_{n=\eta_1}^{\eta_2} K_{m,n} C_n = \lambda_p C_m. \tag{65}$$

with

$$K_{m,n} = -\frac{1}{N} \begin{cases} \frac{\sin(2\nu\sqrt{1+\epsilon^2}\sin(\frac{(m+n)\pi}{N}+\xi)\sin(\frac{(m-n)\pi}{N}))}{\sin(\frac{(m-n)\pi}{N})} & \text{if } m \neq n, \\ 2\nu\sqrt{1+\epsilon^2}\sin(\frac{2n\pi}{N}+\xi) & \text{if } m = n, \end{cases}$$
(66)

where the indexes m, n run from  $\eta_1$  to  $\eta_2$ . This eigenvalue equation (65) can be connected to its continuous counterpart [23] using

$$N = \frac{L}{(\Delta x)} \tag{67}$$

and taking the limit  $(\Delta x) \to 0$ .

We solve numerically the eigenvalue problem of eq. (65) in the same way as we did for the infinite chain case. Our results are shown in figure (5). There we display the maximum eigenvalue  $\lambda_p$  for several values of  $\epsilon$ , highlighting  $c_{\rm BM}$  and  $c_{\rm ring}^{\rm cont}$ , increasing the size of the lattice by an order of magnitude in each figure. We note that as the number of sites increases, the figures resembles to some extent those reported by Goussev [23]. The curve for  $\epsilon = 0$ exhibits the largest value of  $\max(\lambda_p)$ , and this value drops as the lattice grows.

Finally, for each given N, we denote by  $c_{\rm ring}^{\rm tb}$  the maximum of the curve  $\max(\lambda_p)$  as a function of  $\nu$  when  $\epsilon=0$ . In fig. (6) we show how  $c_{\rm ring}^{\rm tb}$  and its corresponding value of  $\nu_{c_{\rm ring}^{\rm tb}}$  depend on N. To establish a clear relationship, we subtract from  $c_{\rm ring}^{\rm tb}$  the value of  $c_{\rm ring}^{\rm cont}=0.11681564947322964$  [23] to which it tends asymptotically as  $N^{-1.7}$  approximately. On the other hand, the right panel shows that to a good approximation,  $\nu_{c_{\rm ring}^{\rm tb}}$  has a dependence of the form  $\sim N^2$  for large N. However, the overall maximum value of  $c_{\rm ring}^{\rm tb}$  for this system is reached when N=5, reaching  $\max(c_{\rm ring}^{\rm tb})\approx 0.131349787116051$ , which is 12% larger than its continuous counterpart  $c_{\rm ring}^{\rm cont}$ .

We also compute the probability flux at j=0 as a function of time for the states that maximize the total backflowing probability, i.e. the solutions to the eigenvalue eqns. (60) and (65). We do this by numerically evaluating the expressions of eqns. (37) and (52). In the left panel we took a  $\nu=50$  for the infinite chain, because in fig.(4), that value corresponds to the point where the oscillations of  $\max(\lambda_p)$  come closest to  $c_{\text{BM}}$ . In the right panel we took  $\nu=26.4$  and N=20 for the periodic chain, this corresponds to the value of  $c_{\text{ring}}^{\text{tb}}$  for this number of sites.

We stress the differences between the backflow discussed in this section and that analyzed in section V. In section V we determine we determine the largest negative flux that can

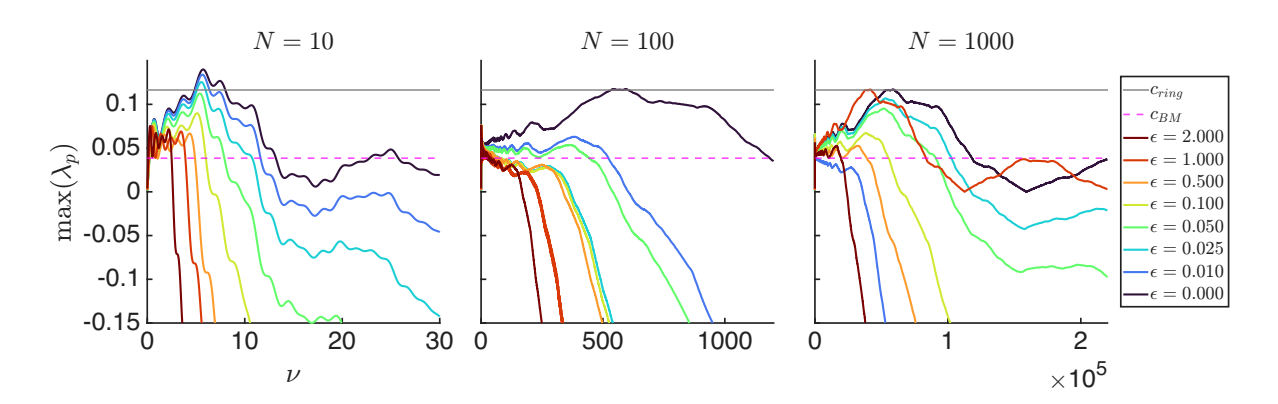


FIG. 5: Maximum of the time negative integrated probability density flux as a function of  $\nu$ , for  $N=10,10^2$  and  $10^3$  sites. The solid gray line corresponds to the result for the continuous version of the system, while the magenta dotted line denotes  $c_{\rm BM}$ . We note that as the number of sites increases, the peak value of the curves converges toward  $c_{\rm ring}^{\rm cont}$  from above, which is in accordance with the scaling law of eq. (67).

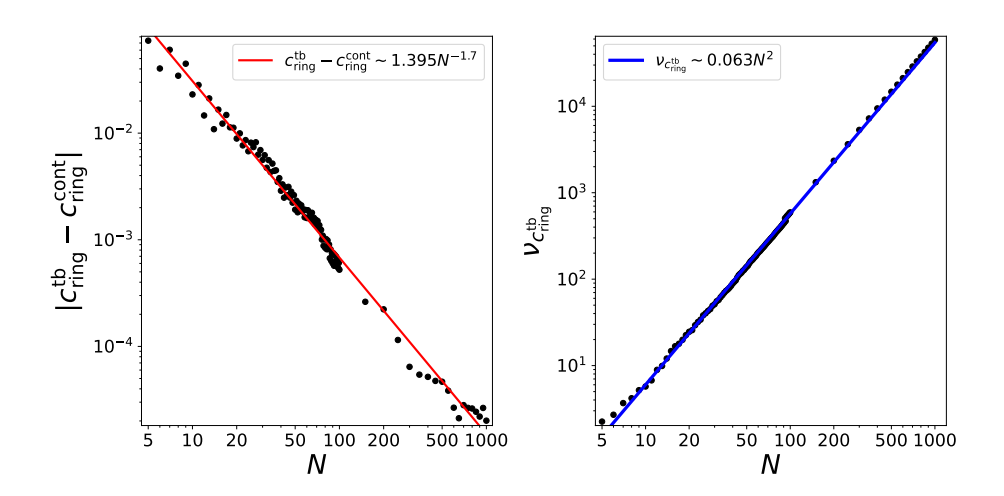


FIG. 6: In the left panel, we show  $c_{\text{ring}}^{\text{tb}} - c_{\text{ring}}^{\text{cont}}$ , and in the right panel the value of  $\nu_{c_{\text{ring}}}^{\text{tb}}$ , both as functions of N. Additionally, we included the fits for the corresponding curves.

appear in these systems, whereas in the Bracken and Melloy approach, we focus on the maximum probability that flows to the left of the origin in a time interval T. This results from a sustained backflowing flux in a time window [-T/2, T/2] with a much more modest amplitude.

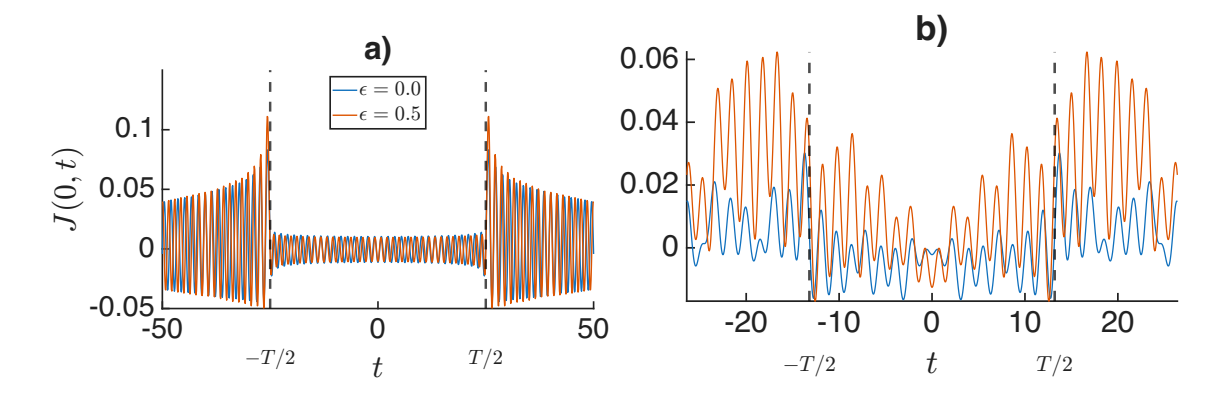


FIG. 7: Probability density flux at j = 0 as function of t, for the infinite chain (a), and the periodic chain with N = 9 (b), with several values  $\epsilon$  using the eigenfunctions appearing in eqns. (60) and (65) respectively. The black dashed lines indicate the limits of the integration time window.

#### VII. CONCLUSIONS AND OUTLOOK

In this work we have described some of the main characteristics of the quantum backflow phenomenon in tight-binding model with complex couplings, both for infinite chains and for periodic chains. These systems display interesting features not only because they broadens the possible experimental approaches in which this effect could be detected and measured, but also from the transport point of view, since it is analogous to classical biased diffusion systems [47–49] or to systems subject to a magnetic field [43]. Actually, the detection of backflow is still an experimental challenge, since it has not been observed in the laboratory, although some experimental proposals have been formulated [50–52]. This has motivated research in quantum backflow to focus on finding configurations that facilitate two aspects: the detection of the effect and the measurement of the quantity  $-\int_{T/2}^{T/2} J(0,t)dt$ . Our present work also aims in this direction: we focused on identifying scenarios in which the negative current is most pronounced and therefore, presumably easier to detect. In this sense, it is similar to the approach used by Palmero et al. [50] in their proposal of an experimental realization based on Bose–Einstein condensates. From this perspective, we found that though it breaks the left-right symmetry in the system, the effect of the bias is essentially to enhance the maximum flux amplitude by factor of  $\sqrt{1+\epsilon^2}$  with respect to the unbiased case. For completeness, we also calculated the upper bounds of the quantity  $-\int_{-T/2}^{T/2} J(0,t), dt$ , and found that they are larger than their continuous counterparts, e.g.,  $c_{\rm BM}=0.0384517$  for a

particle in an infinite line [2] vs 0.0764734 for the infinite chain, whereas for the periodic chains, this quantity depends on the number of sites, being larger for small lattice sizes and  $\epsilon = 0$ . Therefore, tight-binding systems may prove to be suitable systems to observe backflow experimentally and open possibilities for future applications based on it.

## Acknowledgments

Francisco Ricardo Torres Arvizu acknowledges support from SECIHTI scholarship number 834573. Hernán Larralde and Francisco Ricardo Torres Arvizu acknowledges the National Autonomous University of México (UNAM) through the Support Program for Research and Technological Innovation Projects (PAPIIT) number IN103724.

#### VIII. APPENDIX

## Appendix A: Derivation of optimal bounds on the flux for the periodic chain

First, we start defining the functional from the expression of the flux at a fixed j', t' and the constraint defined by the normalization condition eq.(51)

$$I_{1}(c_{m}^{*},c_{n}) = \frac{2\tau\sqrt{1+\epsilon^{2}}}{N\hbar} \sum_{n=\eta_{1}}^{\eta_{2}} \sum_{m=\eta_{1}}^{\eta_{2}} \sum_{m=\eta_{1}}^{\eta_{2}} c_{m}^{*} c_{n} e^{i\left(\frac{(2j'-1)(m-n)\pi}{N} - \frac{(E_{n}-E_{m})t'}{\hbar}\right)} \sin\left(\frac{(m+n)\pi}{N} + \xi\right) - \lambda \sum_{m=\eta_{1}}^{\eta_{2}} |c_{m}|^{2} \tag{A1}$$

Thus, we obtain the Euler-Lagrange equations associated with the last functional

$$\frac{2\tau\sqrt{1+\epsilon^2}}{N\hbar} \sum_{n=n_1}^{\eta_2} c_n e^{i\left(\frac{(2j'-1)(m-n)\pi}{N} - \frac{(E_n - E_m)t'}{\hbar}\right)} \sin\left(\frac{(m+n)\pi}{N} + \xi\right) = \lambda c_m \tag{A2}$$

expanding we have

$$\frac{2\tau\sqrt{1+\epsilon^2}}{N\hbar}e^{-i\left(\frac{(2j'-1)m\pi}{N} - \frac{E_m)t'}{\hbar}\right)} \left[\cos\left(\frac{m}{N}\pi + \frac{\xi}{2}\right)\sum_{n=\eta_1}^{\eta_2}c_n e^{i\left(\frac{(2j'-1)n\pi}{N} - \frac{E_nt'}{\hbar}\right)}\sin\left(\frac{n}{N}\pi + \frac{\xi}{2}\right) + \sin\left(\frac{m}{N}\pi + \frac{\xi}{2}\right)\sum_{n=\eta_1}^{\eta_2}c_n e^{i\left(\frac{(2j'-1)n\pi}{N} - \frac{E_nt'}{\hbar}\right)}\cos\left(\frac{n}{N}\pi + \frac{\xi}{2}\right)\right] = \lambda c_m$$
(A3)

To solve the last equation, we set

$$\sum_{n=\eta_1}^{\eta_2} c_n e^{i\left(\frac{(2j'-1)n\pi}{N} - \frac{E_n t'}{\hbar}\right)} \sin\left(\frac{n}{N}\pi + \frac{\xi}{2}\right) = \alpha$$

$$\sum_{n=n}^{\eta_2} c_n e^{i\left(\frac{(2j'-1)n\pi}{N} - \frac{E_n t'}{\hbar}\right)} \cos\left(\frac{n}{N}\pi + \frac{\xi}{2}\right) = \beta$$
(A4)

therefore

$$c_m = \frac{2\tau\sqrt{1+\epsilon^2}}{N\hbar\lambda}e^{-i\left(\frac{(2j'-1)m\pi}{N} - \frac{E_m)t'}{\hbar}\right)} \left[\alpha\cos\left(\frac{m}{N}\pi + \frac{\xi}{2}\right) + \beta\sin\left(\frac{m}{N}\pi + \frac{\xi}{2}\right)\right]. \tag{A5}$$

Substituting eq. (A5) in eqns. (A4) we get

$$\frac{2\tau\sqrt{1+\epsilon^2}}{N\hbar\lambda} \sum_{n=\eta_1}^{\eta_2} \left[ \alpha \cos\left(\frac{n}{N}\pi + \frac{\xi}{2}\right) + \beta \sin\left(\frac{n}{N}\pi + \frac{\xi}{2}\right) \right] \sin\left(\frac{n}{N}\pi + \frac{\xi}{2}\right) = \alpha$$

$$\frac{2\tau\sqrt{1+\epsilon^2}}{N\hbar\lambda} \sum_{n=\eta_1}^{\eta_2} \left[ \alpha \cos\left(\frac{n}{N}\pi + \frac{\xi}{2}\right) + \beta \sin\left(\frac{n}{N}\pi + \frac{\xi}{2}\right) \right] \cos\left(\frac{n}{N}\pi + \frac{\xi}{2}\right) = \beta$$
(A6)

thus, we obtain the eigenvalue equation

$$\mathbf{A} \begin{pmatrix} \alpha \\ \beta \end{pmatrix} = \lambda \begin{pmatrix} \alpha \\ \beta \end{pmatrix} \tag{A7}$$

where the matrix A has the entries

$$A_{1,1} = A_{2,2} = \frac{\tau\sqrt{1+\epsilon^2}}{N\hbar} \csc\left(\frac{\pi}{N}\right) \sin\left(\frac{\pi(\eta_2+1-\eta_1)}{N}\right) \sin\left(\frac{\pi(\eta_1+\eta_2)}{N}+\xi\right),\tag{A8}$$

$$A_{1,2} = \frac{\tau\sqrt{1+\epsilon^2}}{N\hbar} \left[\eta_2 + 1 - \eta_1 - \cos\left(\frac{\pi(\eta_1 + \eta_2)}{N} + \xi\right) \csc\left(\frac{\pi}{N}\right) \sin\left(\frac{\pi(\eta_2 + 1 - \eta_1)}{N}\right)\right],\tag{A9}$$

$$A_{2,1} = \frac{\tau\sqrt{1+\epsilon^2}}{N\hbar} \left[\eta_2 + 1 - \eta_1 + \cos\left(\frac{\pi(\eta_1 + \eta_2)}{N} + \xi\right) \csc\left(\frac{\pi}{N}\right) \sin\left(\frac{\pi(\eta_2 + 1 - \eta_1)}{N}\right)\right] \tag{A10}$$

and its eigenvalues are

$$\lambda_{\pm} = \frac{\tau\sqrt{1+\epsilon^2}}{N\hbar} \left[ \csc\left(\frac{\pi}{N}\right) \sin\left(\frac{\pi(\eta_2+1-\eta_1)}{N}\right) \sin\left(\frac{\pi(\eta_1+\eta_2)}{N}+\xi\right) \\ \pm \sqrt{(\eta_2+1-\eta_1)^2 - \left(\cos\left(\frac{\pi(\eta_1+\eta_2)}{N}+\xi\right) \csc\left(\frac{\pi}{N}\right) \sin\left(\frac{\pi(\eta_2+1-\eta_1)}{N}\right)\right)^2} \right].$$
(A11)

The relation between  $\alpha$  and  $\beta$  is

$$\alpha = \pm \beta \sqrt{\frac{\eta_2 + 1 - \eta_1 - \cos\left(\frac{\pi(\eta_1 + \eta_2)}{N} + \xi\right) \csc\left(\frac{\pi}{N}\right) \sin\left(\frac{\pi(\eta_2 + 1 - \eta_1)}{N}\right)}{\eta_2 + 1 - \eta_1 + \cos\left(\frac{\pi(\eta_1 + \eta_2)}{N} + \xi\right) \csc\left(\frac{\pi}{N}\right) \sin\left(\frac{\pi(\eta_2 + 1 - \eta_1)}{N}\right)}}.$$
(A12)

Finally, from normalization, we get

$$\beta = \sqrt{\frac{\eta_2 + 1 - \eta_1 + \cos\left(\frac{\pi(\eta_1 + \eta_2)}{N} + \xi\right)\csc\left(\frac{\pi}{N}\right)\sin\left(\frac{\pi(\eta_2 + 1 - \eta_1)}{N}\right)}{\mathcal{D}_{\pm}}}$$
(A13)

where

$$\mathcal{D}_{\pm} = (\eta_2 + 1 - \eta_1)^2 - \cos^2\left(\frac{\pi(\eta_1 + \eta_2)}{N} + \xi\right) \csc^2\left(\frac{\pi}{N}\right) \sin^2\left(\frac{\pi(\eta_2 + 1 - \eta_1)}{N}\right) \\ \pm \csc\left(\frac{\pi}{N}\right) \sin\left(\frac{\pi(\eta_2 + 1 - \eta_1)}{N}\right) \sqrt{(\eta_2 + 1 - \eta_1)^2 - \cos^2\left(\frac{\pi(\eta_1 + \eta_2)}{N} + \xi\right) \csc^2\left(\frac{\pi}{N}\right) \sin^2\left(\frac{\pi(\eta_2 + 1 - \eta_1)}{N}\right)} \sin\left(\frac{\pi(\eta_1 + \eta_2)}{N} + \xi\right). \tag{A14}$$

- [1] G.R. Allcock. The time of arrival in quantum mechanics i. formal considerations. *Annals of Physics*, 53(2):253–285, 1969.
- [2] A J Bracken and G F Melloy. Probability backflow and a new dimensionless quantum number.

  Journal of Physics A: Mathematical and General, 27(6):2197, mar 1994.
- [3] Markus Penz, Gebhard Grübl, Sabine Kreidl, and Peter Wagner. A new approach to quantum backflow. *Journal of Physics A: Mathematical and General*, 39(2):423, dec 2005.
- [4] Simon P. Eveson, Christopher J. Fewster, and Rainer Verch. Quantum inequalities in quantum mechanics. *Annales Henri Poincaré*, 6(1):1–30, 2005.
- [5] S. V. Mousavi and S. Miret-Artés. Dissipative quantum backflow. The European Physical Journal Plus, 135(3):324, 2020.
- [6] Arseni Goussev. Equivalence between quantum backflow and classically forbidden probability flow in a diffraction-in-time problem. *Phys. Rev. A*, 99:043626, Apr 2019.
- [7] G.F. Melloy and A.J. Bracken. The velocity of probability transport in quantum mechanics.

  Annalen der Physik, 510(7-8):726-731, 1998.
- [8] Arseni Goussev. Probability backflow for correlated quantum states. Phys. Rev. Res., 2:033206, Aug 2020.
- [9] J Ashfaque, J Lynch, and P Strange. Relativistic quantum backflow. *Physica Scripta*, 94(12):125107, oct 2019.
- [10] Henning Bostelmann, Daniela Cadamuro, and Gandalf Lechner. Quantum backflow and scattering. *Phys. Rev. A*, 96:012112, Jul 2017.
- [11] Maximilien Barbier. Quantum backflow for many-particle systems. *Phys. Rev. A*, 102:023334, Aug 2020.
- [12] M V Berry. Quantum backflow, negative kinetic energy, and optical retro-propagation. *Journal of Physics A: Mathematical and Theoretical*, 43(41):415302, sep 2010.
- [13] W. van Dijk and F. M. Toyama. Decay of a quasistable quantum system and quantum backflow. Phys. Rev. A, 100:052101, Nov 2019.
- [14] P Strange. Quantum backflow for a free-particle hermite wavepacket. *Physica Scripta*, 99(2):025017, jan 2024.
- [15] Timothy B Boykin and Gerhard Klimeck. The discretized schrödinger equation and simple

- models for semiconductor quantum wells. European Journal of Physics, 25(4):503, may 2004.
- [16] N.W. Ashcroft and N.D. Mermin. Solid State Physics. Cengage Learning, 2011.
- [17] Alexander Szameit and Stefan Nolte. Discrete optics in femtosecond-laser-written photonic structures. Journal of Physics B: Atomic, Molecular and Optical Physics, 43(16):163001, jul 2010.
- [18] S. Longhi. Quantum-optical analogies using photonic structures. Laser & Photonics Reviews, 3(3):243–261, 2009.
- [19] Yang Chen, Xiaoman Chen, Xifeng Ren, Ming Gong, and Guang-can Guo. Tight-binding model in optical waveguides: Design principle and transferability for simulation of complex photonics networks. *Phys. Rev. A*, 104:023501, Aug 2021.
- [20] Falk Lederer, George I. Stegeman, Demetri N. Christodoulides, Gaetano Assanto, Moti Segev, and Yaron Silberberg. Discrete solitons in optics. *Physics Reports*, 463(1):1–126, 2008.
- [21] Yaron Bromberg, Yoav Lahini, Roberto Morandotti, and Yaron Silberberg. Quantum and classical correlations in waveguide lattices. *Phys. Rev. Lett.*, 102:253904, Jun 2009.
- [22] Alberto Peruzzo, Mirko Lobino, Jonathan C. F. Matthews, Nobuyuki Matsuda, Alberto Politi, Konstantinos Poulios, Xiao-Qi Zhou, Yoav Lahini, Nur Ismail, Kerstin Wörhoff, Yaron Bromberg, Yaron Silberberg, Mark G. Thompson, and Jeremy L. OBrien. Quantum walks of correlated photons. Science, 329(5998):1500–1503, 2010.
- [23] Arseni Goussev. Quantum backflow in a ring. Phys. Rev. A, 103:022217, Feb 2021.
- [24] P Strange. Large quantum probability backflow and the azimuthal angle–angular momentum uncertainty relation for an electron in a constant magnetic field. *European Journal of Physics*, 33(5):1147, jul 2012.
- [25] Hong-Yi Su and Jing-Ling Chen. Quantum backflow in solutions to the dirac equation of the spin-1 2 free particle. *Modern Physics Letters A*, 33(32):1850186, 2018.
- [26] Leonardo Di Bari, Valentin Daniel Paccoia, Orlando Panella, and Pinaki Roy. Quantum backflow for a massless dirac fermion on a ring. *Physics Letters A*, 474:128831, 2023.
- [27] Maximilien Barbier and Arseni Goussev. Quantum backflow for two identical particles. *New Journal of Physics*, 27(3):033011, mar 2025.
- [28] Arseni Goussev, Felix Quinque, Jaewoo Joo, and Andrew Burbanks. Quantum backflow current in a ring: Optimal bounds and fractality. *Phys. Rev. A*, 110:022216, Aug 2024.
- [29] Valentin Daniel Paccoia, Orlando Panella, and Pinaki Roy. Angular momentum quantum

- backflow in the noncommutative plane. Phys. Rev. A, 102:062218, Dec 2020.
- [30] Maximilien Barbier, Arseni Goussev, and Shashi C. L. Srivastava. Unbounded quantum backflow in two dimensions. *Phys. Rev. A*, 107:032204, Mar 2023.
- [31] Santiago Rojas-Rojas, Camila Muñoz, Edgar Barriga, Pablo Solano, Aldo Delgado, and Carla Hermann-Avigliano. Analytic evolution for complex coupled tight-binding models: Applications to quantum light manipulation. *Phys. Rev. Res.*, 6:033224, Aug 2024.
- [32] Takahiro Fukui. Theory of edge states based on the hermiticity of tight-binding hamiltonian operators. *Phys. Rev. Res.*, 2:043136, Oct 2020.
- [33] W.G. Kelley and A.C. Peterson. *Difference Equations: An Introduction with Applications*. Harcourt/Academic Press, 2001.
- [34] M. Cruz, M. R. Beltrán, C. Wang, J. Tagüeña Martínez, and Yuri G. Rubo. Supercell approach to the optical properties of porous silicon. *Phys. Rev. B*, 59:15381–15387, Jun 1999.
- [35] B. Gu, N. H. Kwong, and R. Binder. Relation between the interband dipole and momentum matrix elements in semiconductors. *Phys. Rev. B*, 87:125301, Mar 2013.
- [36] M. S. Si and G. P. Zhang. Revisiting the matrix elements of the position operator in the crystal momentum representation. *Europhysics Letters*, 149(2):26001, jan 2025.
- [37] J.J. Sakurai and J. Napolitano. Modern Quantum Mechanics. Cambridge University Press, 2017.
- [38] Thomas Garm Pedersen, Kjeld Pedersen, and Thomas Brun Kriestensen. Optical matrix elements in tight-binding calculations. *Phys. Rev. B*, 63:201101, May 2001.
- [39] Chi-Cheng Lee, Yung-Ting Lee, Masahiro Fukuda, and Taisuke Ozaki. Tight-binding calculations of optical matrix elements for conductivity using nonorthogonal atomic orbitals:

  Anomalous hall conductivity in bcc fe. *Phys. Rev. B*, 98:115115, Sep 2018.
- [40] Timothy B. Boykin and P. Vogl. Dielectric response of molecules in empirical tight-binding theory. *Phys. Rev. B*, 65:035202, Dec 2001.
- [41] G.H. Weiss. Aspects and Applications of the Random Walk. International Congress Series. North-Holland, 1994.
- [42] Norio Inui. Continuous limit of a tight-binding model on a hexagonal disk in a magnetic field: size dependence on energy level. *Physica Scripta*, 98(10):105254, sep 2023.
- [43] G A Vugalter, A K Das, and V A Sorokin. A charged particle on a ring in a magnetic field: quantum revivals. *European Journal of Physics*, 25(2):157, dec 2003.

- [44] Gerald Rosen. Galilean invariance and the general covariance of nonrelativistic laws. *American Journal of Physics*, 40(5):683–687, 05 1972.
- [45] Daniel M. Greenberger. Inadequacy of the usual galilean transformation in quantum mechanics. *Phys. Rev. Lett.*, 87:100405, Aug 2001.
- [46] Abdul-Majid Wazwaz. Linear and nonlinear integral equations, volume 639. Springer, 2011.
- [47] Zoltán Zimborás, Mauro Faccin, Zoltán Kádár, James D. Whitfield, Ben P. Lanyon, and Jacob Biamonte. Quantum transport enhancement by time-reversal symmetry breaking. Scientific Reports, 3(1):2361, 2013.
- [48] Dawei Lu, Jacob D. Biamonte, Jun Li, Hang Li, Tomi H. Johnson, Ville Bergholm, Mauro Faccin, Zoltán Zimborás, Raymond Laflamme, Jonathan Baugh, and Seth Lloyd. Chiral quantum walks. Phys. Rev. A, 93:042302, Apr 2016.
- [49] Yang Liu and D. L. Zhou. Quantum state transfer along a ring with time-reversal asymmetry. *Phys. Rev. A*, 91:052318, May 2015.
- [50] M. Palmero, E. Torrontegui, J. G. Muga, and M. Modugno. Detecting quantum backflow by the density of a bose-einstein condensate. *Phys. Rev. A*, 87:053618, May 2013.
- [51] J. M. Yearsley, J. J. Halliwell, R. Hartshorn, and A. Whitby. Analytical examples, measurement models, and classical limit of quantum backflow. *Phys. Rev. A*, 86:042116, Oct 2012.
- [52] Maximilien Barbier and Arseni Goussev. On the experiment-friendly formulation of quantum backflow. *Quantum*, 5:536, September 2021.